Pergamon

Int. J. Solids Structures Vol. 35, No. 7–8, pp. 701–717, 1998

0020–7683/98 $19.00 + .00

PII: S0020–7683(97)00082–6

CRACK BRIDGING IN FUNCTIONALLY GRADED COATINGS

H. CAI and G. BAO†
Department of Mechanical Engineering, The Johns Hopkins University, Baltimore, MD 21218, U.S.A.

(*Received* 12 *July* 1996; *in revised form* 24 *February* 1997)

Abstract—A crack bridging analysis is carried out to predict crack propagation in coatings made of functionally graded materials (FGM). The FGM coating is taken to be a ceramic/metal composite with its gradation characterized by the local volume fractions of metal and ceramic phases. Fracture in the FGM coating is resisted by the plastic deformation of metal ligaments in the crack wake that bridge the crack; the crack bridging, however, is not uniform. A position-dependent crack bridging model is developed taking into account the coating gradation and metal plasticity. The model is subsequently used in a finite element analysis to predict the reduced fracture driving force. It is found that crack bridging in the FGM coating can significantly reduce the crack tip stress intensity. It is also found that coating gradation has a strong influence on the fracture driving force and the crack length at arrest. The present finite element model can be extended readily to study the effect of large-scale plastic deformation on crack growth in a FGM coating. © 1997 Elsevier Science Ltd

1. INTRODUCTION

Functionally graded materials (FGMs) have the potential to enjoy a wide range of thermal and structural applications, including thermal gradient structures, wear and corrosion resistant coatings and metal/ceramic joining (Takahashi and Hashida, 1990; Mortensen and Suresh, 1995). To establish the fundamental relationship between material gradation and thermomechanical properties of FGMs, extensive studies have been carried out of the effective properties (Aboudi *et al.* 1994; Dvorak and Zuiker, 1994; Aboudi *et al.* 1995), deformation and stress distributions (Williamson *et al.*, 1993; Drake *et al.*, 1993; Giannakopoulos *et al.*, 1995; Finot and Suresh, 1996) and fracture in functionally graded materials (Erdogan, 1985; Delale and Erdogan, 1983, 1988; Erdogan and Wu, 1993; Chen and Erdogan, 1996). In particular, the fracture mechanics analysis of Erdogan and associates has been extended by Noda and Jin to include thermal load (Jin and Noda, 1993; Noda and Jin, 1993; Jin and Noda, 1994), and by Bao and Wang (1995) and Bao and Cai (1996) to include the effects of different material gradation. Experimental observations of cracking in FGMs have been made by several investigators, including surface crack initiation in thermal barrier coatings (Kokini and Takeuchi, 1994) and multiple cracking in a NiAl-Al_2O_3 FGM layer under bending (Lannutti, 1994).

Ceramic, metal and polymer coatings have been widely used in various industries, from aerospace to automobile to microelectronics, to enhance the performance. In particular, ceramic coatings have been developed for use in thermal gradient structures, automotive engines and cutting and grinding tools to protect the surfaces from melting, wear, corrosion and oxidation. However, due to thermal expansion mismatch between the coating and substrate, multiple cracking and coating spalling can occur upon experiencing thermal cycling and mechanical loading, causing premature failure of the component. The use of functionally graded coatings has the potential to simultaneously reduce thermal expansion mismatch, increase interface bonding strength, and enhance coating toughness. To realize this potential, a systematic micromechanics study was carried out by Bao and Wang (1995) of multiple cracking in functionally graded ceramic/metal coatings. Systematic finite element calculations were made for the energy release rate of the cracks in the coating as

† Correspondence address: Department of Mechanical Engineering, The Johns Hopkins University, 125 Latrobe Hall 3400 N. Charles St., Baltimore MD 21218-2686, U.S.A.

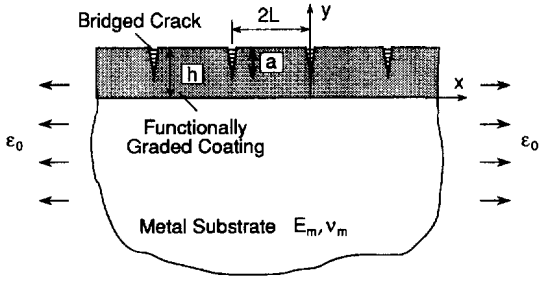

Fig. 1. A schematic of bridged multiple cracks in a functionally graded coating/metal-substrate system.

determined by the coating gradation, crack length, and the crack density; both mechanical and thermal loads were considered. However, in their study, the influence of crack bridging and metal plasticity in the functionally graded coatings was neglected.

Crack bridging is a very common phenomenon in the fracture of composites (Bao and Suo, 1992). For example, in a unidirectional ceramic fiber reinforced metal matrix composite, fibers can bridge the matrix crack, reducing the crack-tip stress intensity, and increasing significantly the fatigue life of the component (Walls *et al.*, 1993; Bao and McMeeking, 1994, 1995). When a ceramic/metal FGM coating is of the inclusion/matrix type, the metal particles in the ceramic matrix can bridge the crack, thus enhance the fracture resistance of the coating. The fracture behavior of ductile-particle reinforced brittle matrix composites has been analyzed (e.g., Bao and Hui, 1990; Bao and Zok, 1993) based on uniform crack bridging models. However, crack bridging in a functionally graded coating is non-uniform, since the local volume fraction of the metal phase changes with position in the coating.

In this study, crack bridging in the FGM coating is analyzed using a position-dependent crack bridging law. Considered is multiple cracking in a ceramic/metal FGM coating perfectly bonded to a homogeneous metal substrate, as depicted in Fig. 1. The coating is taken to be a composite with the local volume fraction of metal varying through the coating thickness according to a power-law type relation. Both the FGM coating and the metal substrate are taken as linear elastic; plastic deformation of the metal phase in the coating is included in the model through the crack bridging analysis. Systematic finite element predictions are made for the fracture driving force of bridged multiple cracks in a FGM coating as determined by the crack bridging characteristics, coating gradation, the crack length and spacing, and the applied load. Assuming the intrinsic toughness of the FGM coating is that of the ceramic phase, the onset of unstable crack growth and the crack arrest are also analyzed.

2. COATING GRADATION AND THE NON-UNIFORM CRACK BRIDGING

Based on the performance requirements for thermal barrier coatings and coatings in wear-related applications, in this study, only coatings that are ceramic-rich near the surface and metal-rich near the coating/substrate interface are considered. For convenience, the y-axis is set along the coating thickness direction, the x-axis lies within the coating/substrate interface, as illustrated in Fig. 1. At any position y in the ceramic/metal coating, the local volume fraction of ceramic is assumed to obey a pure power-law relation $g(y)$

$$g(y) = (y/h)^n \tag{1}$$

where the exponent n is a material parameter. The gradation given in (1) implies that the coating always has 100% ceramic at the coating surface (i.e., $g(h) = 1$) and 100% metal at the interface (i.e., $g(0) = 0$). The local volume fraction of metal $f(y)$ is given by

$$f(y) = 1-g(y) = 1-(y/h)^n \tag{2a}$$

and the total volume fraction of metal f_m in the coating is related to the exponent n in (1) by

$$f_m = n/(n+1). \tag{2b}$$

Due to the heterogeneous nature of a functionally graded material, it is quite difficult to obtain exact solutions of the effective elastic moduli of a FGM coating in terms of the relative volume fractions and elastic properties of the metal and ceramic phases. For a FGM coating of the inclusion/matrix type, the microgeometry of each phase is usually irregular, the spatial distribution of the phases is not uniform along the y-direction, and the homogenization can only be made within a plane parallel to the x-axis. Consequently, the existing micromechanical cell models are no longer valid since no unit cell containing a single inclusion can be used to represent the whole composite body. Even if one chooses a unit cell containing many particles aligned along the coating thickness direction, due to the finite thickness of the coating, there is a particle-size dependence of the unit cell. A robust micromechanical model for the thermomechanical properties of a functionally graded coating is yet to be developed (Markworth *et al.*, 1995).

As a first-order approximation, in this study, Young's modulus $E(y)$ and Poisson's ratio $v(y)$ of the FGM coating are obtained using micromechanics models developed for composites with homogeneously distributed spherical reinforcements. The effective bulk modulus $k(y)$ of the coating can be expressed as (Hashin, 1962)

$$k(y) = k_m + \frac{g(y)(k_c-k_m)}{1+[1-g(y)][(k_c-k_m)/(k_m+\frac{4}{3}\mu_m)]} \tag{3}$$

where k_m and k_c are bulk moduli for metal and ceramic, respectively, and μ_m is the shear modulus for the metal phase. The effective shear modulus $\mu(y)$ of the coating can be solved from (Christensen and Lo, 1979)

$$A\left[\frac{\mu(y)}{\mu_m}\right]^2 + B\left[\frac{\mu(y)}{\mu_m}\right] + C = 0 \tag{4}$$

where A, B and C are functions of $g(y)$, μ_c/μ_m, v_c and v_m (Poisson's ratios for ceramic and metal, respectively) given in Christensen and Lo (1979), and μ_c is the shear modulus for the ceramic phase. The effective Young's modulus $E(y)$ and Poisson's ratio $v(y)$ are given in terms of $k(y)$ and $\mu(y)$ by

$$E(y) = \frac{9k(y)\mu(y)}{3k(y)+\mu(y)}, \quad v(y) = \frac{E(y)}{2\mu(y)} - 1. \tag{5}$$

For a FGM coating that is ceramic-rich near the surface, cracks perpendicular to the interface can initiate at the coating surface and propagate into the coating under applied thermal or mechanical tensile loads (Lannutti, 1994). These cracks may be bridged by the

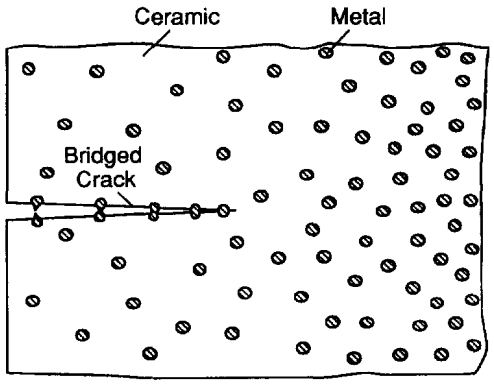

Fig. 2. A schematic of position-dependent crack bridging in functionally graded materials.

metal particle in the FGM coating, as shown schematically in Fig. 2. As a consequence of metal volume fraction variation in the FGM coating, the bridging traction on the crack surfaces provided by metal particles is position-dependent (Fig. 2). At a fixed location, the bridging-stress versus crack-opening curve for a single ductile particle bridging the matrix crack in its wake is typically as the solid line shown in Fig. 3a (Ashby *et al.*, 1989). To simplify the analysis and at the same time capture the essence of the bridging mechanism, in this study, an idealized rectilinear bridging law (Bao and Suo, 1992) shown as the dashed line in Fig. 3a will be used. Specifically, the rectilinear bridging law $\sigma(\delta)$ is characterized by two parameters σ_0 and δ_0

$$\sigma = \sigma_0, \quad 0 \leqslant \delta < \delta_0; \tag{6a}$$

$$\sigma = 0, \quad \sigma > \delta_0. \tag{6b}$$

In eqn (6), δ_0 can be chosen as the limiting separation of the crack surfaces beyond which the metal particle will rupture, and the bridging strength σ_0 can be given from the following energy-balance equation

$$\sigma_0 \delta_0 = \int_0^{\delta_0} \sigma(\delta)\, \mathrm{d}\delta \tag{6c}$$

where the function $\sigma(\delta)$ is the measured crack bridging curve shown as the solid line in Fig. 3a. In general, σ_0 depends on the plastic flow behavior and shape of the metal particles, and the particle/matrix interface strength (Mataga, 1989).

The crack bridging law given in (6) is for a single metal particle that bridges the crack. The crack bridging law shown in Fig. 3b for the entire bridging zone is obtained by smearing out the stresses in the bridging particles according to the local volume fraction of metal in the FGM coating

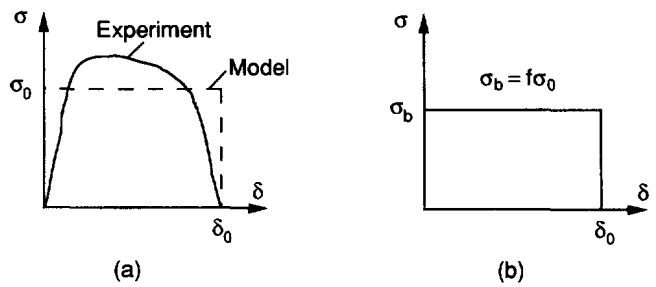

Fig. 3. The crack bridging law (a) for a single metal particle in the bridging zone; (b) for the FGM coating where f is the local volume fraction of the metal phase.

$$\sigma = \sigma_b, \quad 0 \leqslant \delta < \delta_0; \tag{7a}$$

$$\sigma = 0, \quad \delta > \delta_0 \tag{7b}$$

where $\sigma_b(y) = f(y)\sigma_0$ is the position-dependent bridging strength

$$\sigma_b(y) = [1-g(y)]\sigma_0 = [1-(y/h)^n]\sigma_0. \tag{7c}$$

In deriving eqn (7), it is assumed that the local area fraction of the bridged particles can be taken as the local volume fraction of metal phase. While not true for all cases, this assumption is valid for a large class of composites.

3. MULTIPLE CRACKING UNDER UNIFORM STRAINING

Analyzed in this section is multiple cracking in the FGM coating/metal substrate system owing to a remotely applied uniform strain ε_0 in the x-direction, as illustrated in Fig. 1. For simplicity, the cracks are taken to be mode I, plane strain, parallel and equally spaced with spacing $2L$, and have the same length. For an uncracked coating/substrate system subjected to ε_0, the stress along the x-direction in the coating is given by

$$\sigma_x(y) = \frac{\varepsilon_0 E(y)}{1-\nu^2(y)} \tag{8}$$

and that in the substrate is uniform

$$\sigma_x = \frac{\varepsilon_0 E_m}{1-\nu_m^2}. \tag{9}$$

The average stress in the x-direction corresponding to the applied strain ε_0 is obtained readily as

$$\sigma = \frac{\varepsilon_0}{h+H}\left[\frac{HE_m}{1-\nu_m^2} + \int_0^h \frac{E(y)}{1-\nu^2(y)}\,\mathrm{d}y\right] \tag{10}$$

where H is the thickness of the substrate. In what follows, this average stress σ, often referred to as the "applied stress", is used to represent the effect of the applied strain ε_0. The energy release rate $\mathscr{G}$ at each tip of the unbridged multiple cracks can be normalized to give

$$\frac{\mathscr{G}\bar{E}_m}{\sigma^2 h} = \psi\left(\frac{a}{h}, \frac{L}{h}, \frac{\delta_0}{h}, \frac{\sigma_0}{E_m}, \frac{\sigma}{E_m}, n\right) \tag{11}$$

where ψ is a non-dimensional function and the dependence of ψ on E_c/E_m, ν_c and ν_m is left implicit. Systematic finite element predictions are made for the energy release rate $\mathscr{G}$ at the tip of the bridged crack varying a/h, L/h, σ_0/E_m, σ/E_m and n. A detailed discussion of these predictions is given in Section 3.3.

3.1. *The finite element model*

Finite element calculations were carried out using the commercial code ABAQUS to obtain the energy release rate $\mathscr{G}$ for bridged multiple cracks in a FGM coating. The coating/substrate system depicted in Fig. 1 is subjected to a remotely applied uniform strain ε_0 in the x-direction. Owing to translational symmetry of the parallel cracks, only a unit

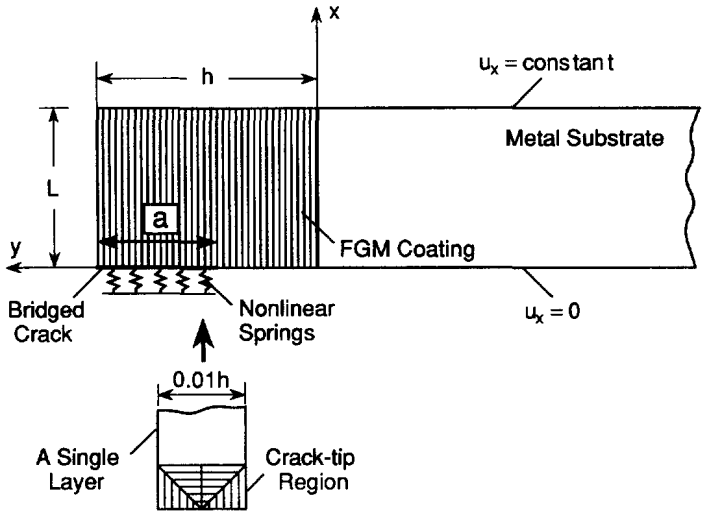

Fig. 4. The unit cell used in the finite element calculations for the bridged multiple cracks in the FGM coating. The coating is divided into 100 layers and the energy release rate is calculated with the crack tip located in the middle of a layer.

cell with width L containing a single crack as shown in Fig. 4 needs to be considered in the finite element calculation. The thickness of the substrate H is taken to be $300h$ where h is the coating thickness. The FGM coating is divided into 100 layers with one element per layer in the thickness direction, each layer is homogeneous, isotropic with elastic moduli $E(y_i)$ and $v(y_i)$ where y_i is the position of the middle plane of the layer measured from the coating/substrate interface ($y = 0$). Clearly, in this finite element model the gradation is not continuous, nor is it in the real material. This model mimics the microstructure of a fine multilayered FGM coating, or an inclusion/matrix type FGM coating with gradation $g(y)$.

As can be seen from Fig. 4, the mode I, plane strain crack lies on $x = 0$, $h-a \leqslant y \leqslant h$. For $-H \leqslant y \leqslant h-a$, the displacement in the x-direction $u_x = 0$. The unit cell is constrained in such a way that the edge $x = L$ has a uniform displacement in the x-direction $u_x = \varepsilon_0 L$, where ε_0 is the applied strain. The energy release rate is calculated with the crack tip located in the middle of a layer, as depicted in Fig. 4. Complications due to the singular behavior at the interfaces of two adjacent layers can thus be avoided. The position-dependent crack bridging is simulated using discrete nonlinear springs attached to the nodes on the crack surfaces and to the symmetry plane $x = 0$. The behavior of the nonlinear springs is defined by the relationship between the force and the relative displacement in the spring, i.e.,

$$P = \begin{cases} A_b\sigma_b = A_b\sigma_0[1-(y_i/h)^n], & \text{when } 0 \leqslant \delta < \delta_0 \\ 0, & \text{when } \delta \geqslant \delta_0 \end{cases} \tag{12}$$

where A_b is the element area (or length in the case of a plane strain problem) associated with the attached spring and y_i is the location of the middle plane of the layer containing the nonlinear spring. In all the finite element calculations, fixed values of $E_c/E_m = 3.0$, $v_c = 0.2$, $v_m = 0.3$, $\delta_0/h = 0.05$ were used. An accuracy check of this finite element crack bridging model has been carried out as discussed below.

3.2. *Validation of the finite element crack bridging model*

In order to check the accuracy of the finite element crack bridging model discussed above, a special case is considered in which the coating is taken to be homogeneous isotropic with elastic moduli identical to that of the substrate. The crack bridging law is taken to be rectilinear as defined in (7a) and (7b) with the position-dependent bridging strength σ_b given by

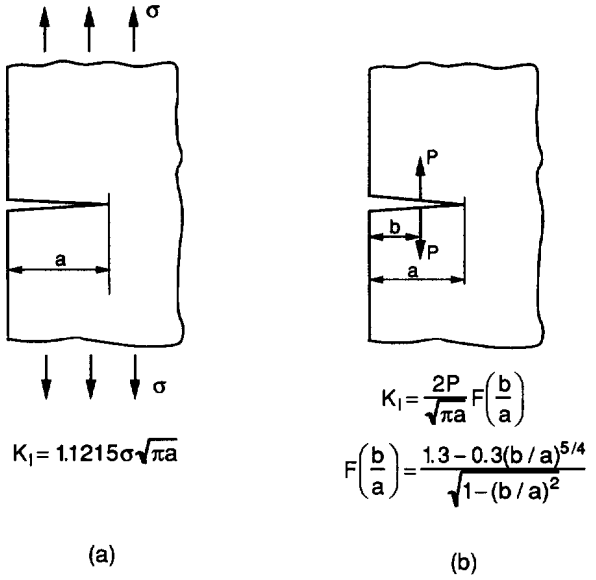

Fig. 5. The stress intensity factor for an edge crack in a semi-infinite homogeneous isotropic body under (a) remotely applied uniform stress and (b) a pair of point loads on the crack surfaces.

$$\sigma_b = (t/h)\sigma_0 \tag{13}$$

where t is the position in the coating measured from the coating surface, and h is the coating thickness. Evidently, eqn (13) is a special case of (7c) with $t = h - y$ and $n = 1$.

For a single unbridged edge crack with length a in a semi-infinite, homogeneous, isotropic body under remotely applied tensile stress σ as depicted in Fig. 5a, the stress intensity factor K_a is given by (Tada *et al.*, 1985)

$$K_a = 1.1215\sigma\sqrt{\pi a}. \tag{14}$$

On the other hand, the stress intensity factor of the crack under a pair of point loads P applied on the crack surfaces a distance b away from the coating surface (Fig. 5b) is given by (Tada *et al.*, 1985)

$$K_I = \frac{2P}{\sqrt{\pi a}} F\left(\frac{b}{a}\right) \tag{15a}$$

where

$$F\left(\frac{b}{a}\right) = \frac{1.3 - 0.3(b/a)^{5/4}}{\sqrt{1-(b/a)^2}}. \tag{15b}$$

The crack-tip stress intensity K_{tip} for a fully bridged crack is thus

$$K_{tip} = 1.1215\sigma\sqrt{\pi a} - \frac{2}{\sqrt{\pi a}} \int_0^a \sigma_b(t) F\left(\frac{t}{a}\right) dt. \tag{16}$$

Substituting (13) into (16) and performing the integration, we have

$$\frac{K_{tip}}{\sigma\sqrt{\pi a}} = \left(1.1215 - \frac{2.15}{\pi} \frac{\sigma_0}{\sigma} \frac{a}{h}\right). \tag{17}$$

In a nondimensional form, the energy release rate $\mathcal{G}$ at the crack-tip can be expressed as

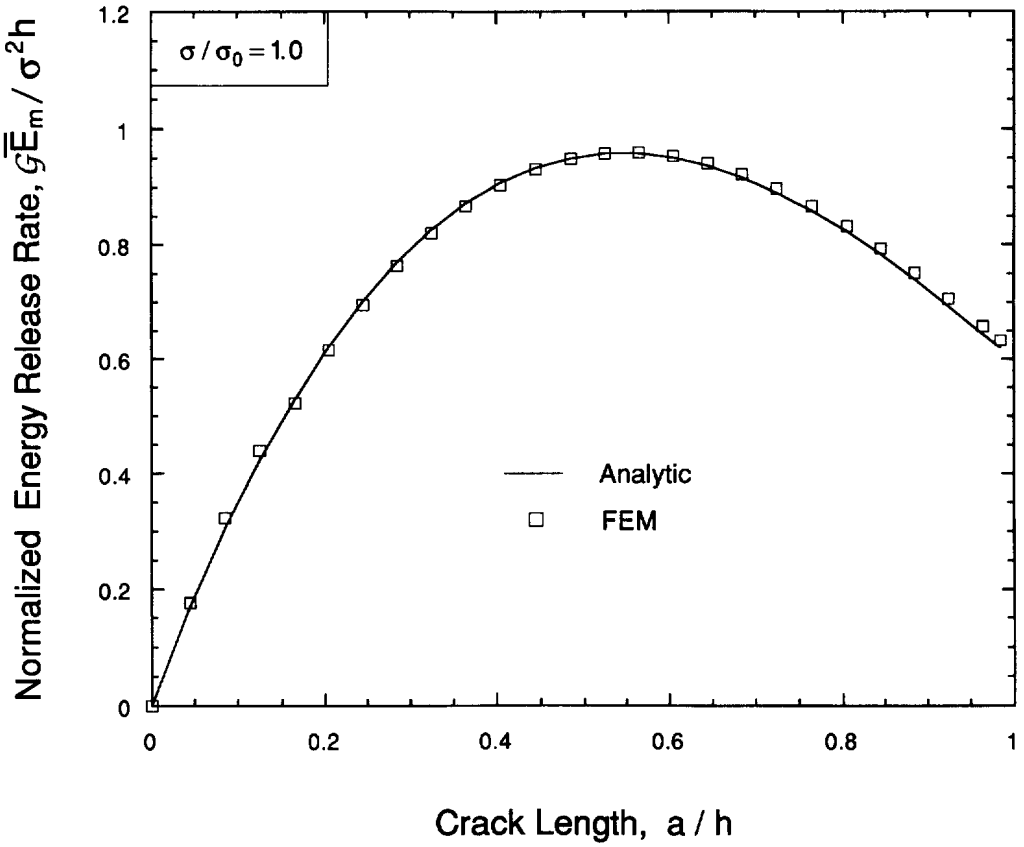

Fig. 6. Comparison of the normalized crack-tip energy release rate as a function of the crack length obtained using the closed-form solution (18) and the finite element crack bridging model.

$$\frac{\mathcal{G}\bar{E}_m}{\sigma^2 h} = \pi\left(1.1215 - \frac{2.15}{\pi}\frac{\sigma_0}{\sigma}\frac{a}{h}\right)^2 \frac{a}{h} \tag{18}$$

where $\bar{E}_m = E_m/(1-\nu_m^2)$ is the plane strain Young's modulus of the substrate.

Plotted in Fig. 6 is the comparison of the normalized energy release rate as a function of the crack length obtained from the closed-form solution (18) and from the finite element calculations with $\sigma_0/E_m = 0.001$ under applied stress $\sigma/E_m = 0.001$. In the finite element calculations, $L/h = 100$, $H/h = 300$ is used. The limiting-separation δ_0 assumed in the crack bridging law is sufficiently large ($\delta_0/h = 0.05$) so that the crack remains fully bridged under the applied load. As can be seen from the comparison shown in Fig. 6, the finite element model is quite accurate in obtaining the energy release rate of a bridged crack.

3.3. *Finite element predictions*

Plotted in Fig. 7 is the normalized energy release rate $\mathcal{G}\bar{E}_m/\sigma^2 h$ as a function of the normalized crack length a/h with $n = 1$, $\sigma_0/E_m = 0.002$, $L/h = 2$ under applied stress $\sigma/E_m = 0.0004$. Corresponding results for multiple cracks in a pure ceramic coating and unbridged cracks in the FGM coating are also shown for comparison. It is clear that FGM coatings can significantly reduce the crack driving force and crack bridging can make the driving force reduction even more pronounced. In particular, for the bridged cracks, the energy release rate versus crack length curve shows a peak indicating that the cracks may arrest at a certain crack length when the fracture driving force falls below the intrinsic toughness of the coating and thereafter, an increased applied load is required to propagate the crack further (stable crack growth). This scenario will be discussed in more detail in Section 4. It is also noteworthy that for the bridged crack, the energy release rate $\mathcal{G}$ at the crack tip goes to zero at about $a = 0.6h$. This is due to the fact that the applied load is

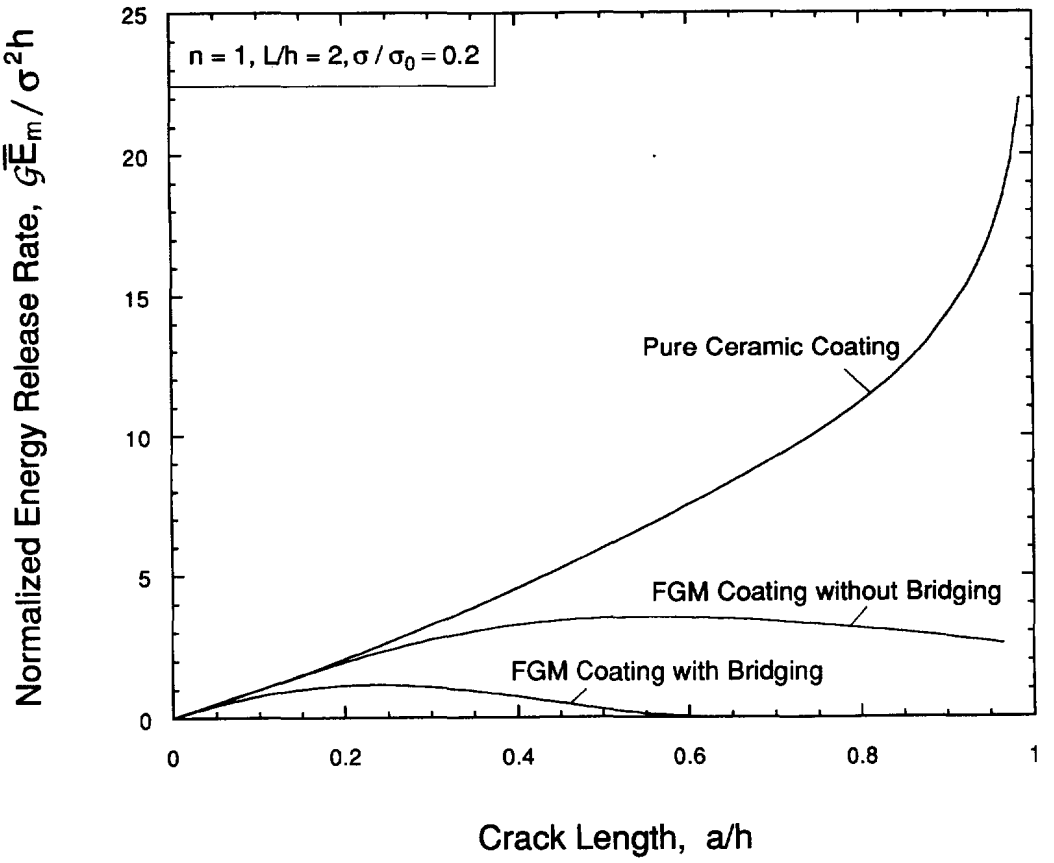

Fig. 7. Comparison of the normalized energy release rates as a function of the crack length for (i) unbridged cracks in a pure ceramic coating; (ii) unbridged cracks in a FGM coating; and (iii) bridged cracks in a FGM coating.

relatively low, and the crack bridging is quite strong; the crack is always fully bridged since the assumed limiting-separation δ_0 is large.

To uncover the influence of coating gradation on the fracture driving force, systematic predictions are made for the energy release rate $\mathcal{G}$ corresponding to different coating gradation $g(y)$. Shown in Fig. 8 are $\mathcal{G}\bar{E}_m/\sigma^2 h$ vs a/h curves for $L/h = 2$, $\sigma_0/E_m = 0.002$, $\sigma/E_m = 0.0005$ for $n = 0.5$, 1 and 2. As expected, there is a strong dependence of $\mathcal{G}$ on the value of gradation exponent n: a large value of n leads to a low energy release rate $\mathcal{G}$. Note that a large n implies a high metal content in the coating, as indicated by eqn (2b).

The effect of bridging strength σ_0 is illustrated in Fig. 9 in which $\mathcal{G}\bar{E}_m/\sigma^2 h$ is plotted as a function of a/h for $n = 1$, $L/h = 2$, $\sigma/E_m = 0.0004$ for $\sigma_0/E_m = 0.001$, 0.002, 0.003. The trend is clear: a high bridging strength σ_0 gives a low fracture driving force. In fact, with a fixed crack opening δ at the coating surface the reduction in crack-tip energy release rate due to plastic deformation of the bridging metal particles is simply proportional to σ_0. Note also that the crack length at which the energy release rate $\mathcal{G}$ approaches zero decreases with increasing σ_0.

Presented in Fig. 10 is $\mathcal{G}\bar{E}_m/\sigma^2 h$ as a function of the crack length a/h for $n = 1$, $\sigma/E_m = 0.0004$, $\sigma_0/E_m = 0.002$ for $L/h = 2$, 5, 10 and 50. The energy release rate $\mathcal{G}$ increases with crack spacing, or in other words, the fracture driving force for each crack is reduced as more and more cracks developed (i.e., L/h becomes smaller). It is interesting to note that when the crack length is small (say, $a/h < 0.2$), the energy release rate is essentially independent of crack spacing. It is also clear that when crack spacing L/h becomes large (say, $L/h > 50$), the interaction between the parallel cracks diminishes, and each crack behaves like an isolated crack. That is the reason behind the saturating trend of the effect of L/h on energy release rate $\mathcal{G}$ as shown in Fig. 10.

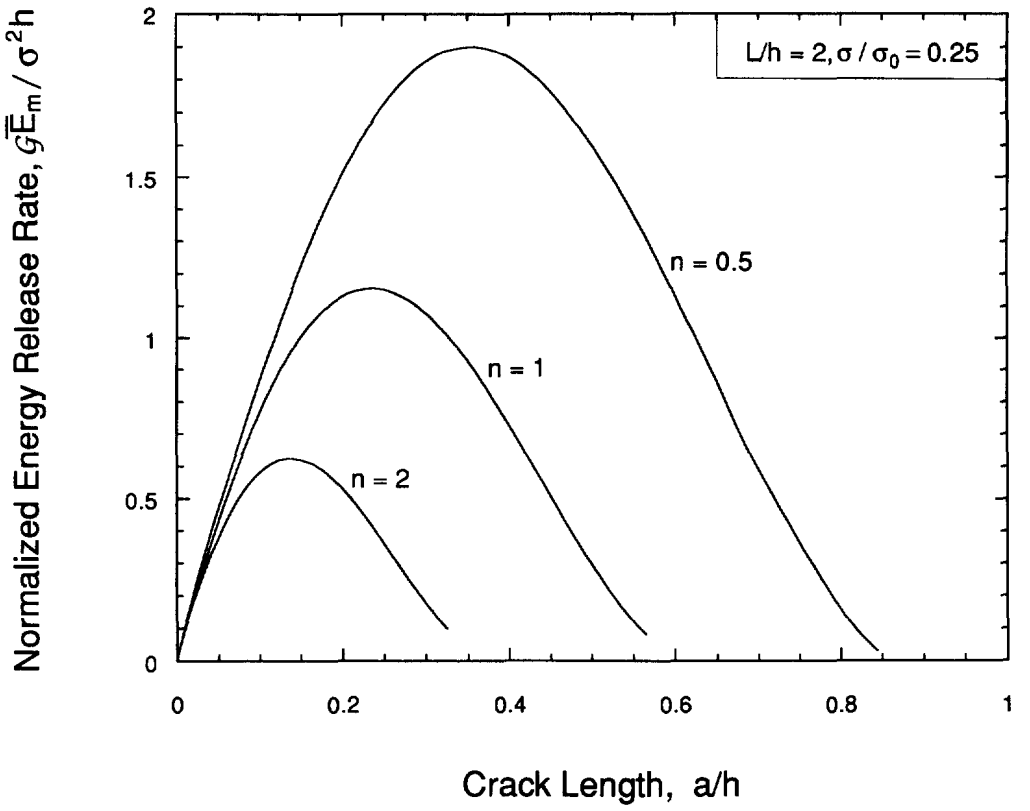

Fig. 8. The normalized energy release rate as a function of the crack length for FGM coatings with $n = 0.5$, 1.0 and 2.0, $L/h = 2$, $\sigma_0/E_m = 0.002$ under applied stress $\sigma/E_m = 0.0004$.

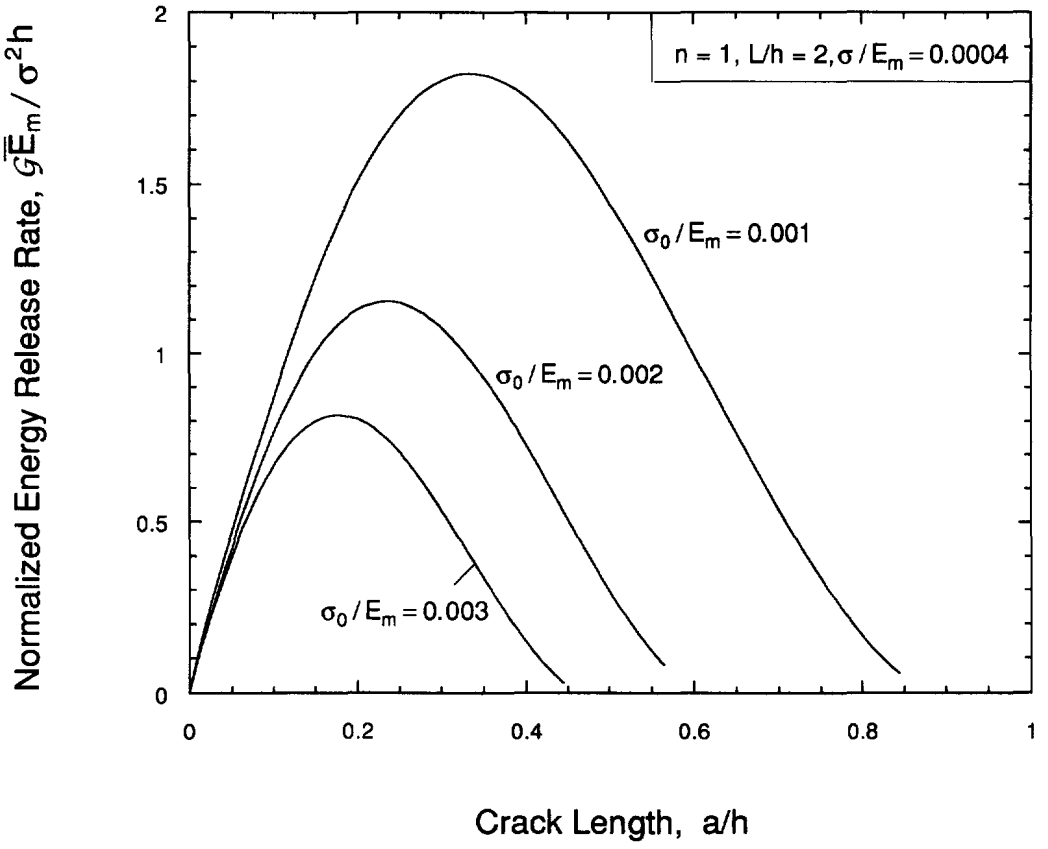

Fig. 9. The normalized energy release rate as a function of the crack length for FGM coatings with $n = 1$, $L/h = 2$, $\sigma_0/E_m = 0.001$, 0.002 and 0.003 under applied stress $\sigma/E_m = 0.0004$.

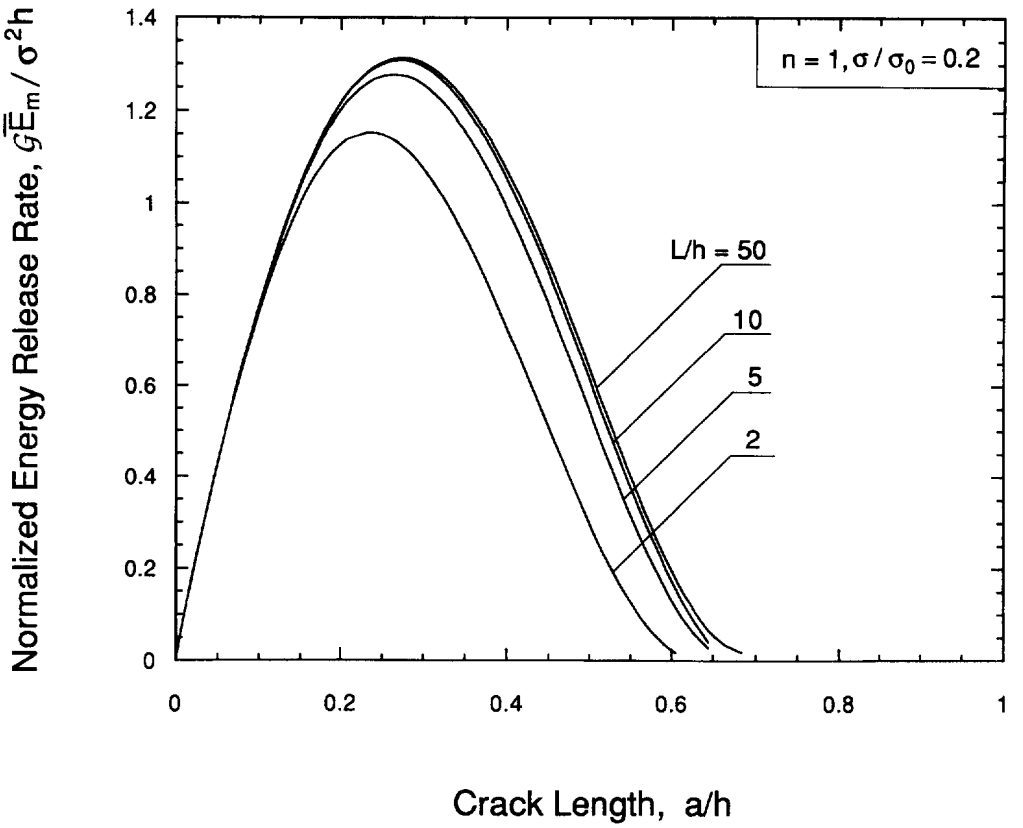

Fig. 10. The normalized energy release rate as a function of the crack length for a FGM coating with $n = 1$, $L/h = 2$, 5, 10 and 50, $\sigma_0/E_m = 0.002$ under applied stress $\sigma/E_m = 0.0004$.

Figure 11 shows the normalized energy release rate $\mathcal{G}\bar{E}_m/\sigma^2 h$ as a function of the crack length a/h for $n = 1$, $L/h = 2$, $\sigma_0/E_m = 0.002$ for different applied load $\sigma/E_m = 0.0003$, 0.0004, 0.0005. Evidently, the fracture driving force $\mathcal{G}$ increases with applied load. However, the crack-tip energy release rate $\mathcal{G}$ does not scale with σ^2 as for an unbridged crack due to the nonlinear feature of the crack bridging and the interplay between crack bridging and the applied load. Otherwise, all the curves shown in Fig. 11 should collapse onto one curve.

The $\mathcal{G}\bar{E}_m/\sigma^2 h$ vs a/h curves shown in Figs 8–11 indicate that, under the given applied far-field uniform strain ε_0, the energy release rate $\mathcal{G}$ at the crack-tip may become zero at certain crack length. This can be understood from the following energy equation

$$\mathcal{G} = \mathcal{G}_{\text{appl}} - \mathcal{G}_b \tag{19}$$

where $\mathcal{G}_{\text{appl}}$ and $\mathcal{G}_b$ are the energy release rates due to the applied strain ε_0 and crack bridging, respectively. Owing to the functional gradation of the coating, for $a/h > 0.2$, $\mathcal{G}_{\text{appl}}$ does not change much with crack length as can be seen from Fig. 7, but $\mathcal{G}_b$ increases as the crack length a increases. At certain crack length say, $a = a_c$, $\mathcal{G}_b$ may become the same as $\mathcal{G}_{\text{appl}}$, which implies that at a_c the crack-tip energy release rate $\mathcal{G}$ is zero.

4. STABLE CRACK GROWTH IN A FGM COATING

As mentioned earlier, the fracture driving force vs crack length curve for bridged multiple cracks in a functionally graded coating has a peak indicating that a crack may initiate at certain crack length and arrest at another under a given applied load. Based on the finite element results for the crack-tip energy release rate discussed in the last section, and the intrinsic toughness of the coating, the crack length at the onset of unstable crack growth and the crack length at arrest can be quantified.

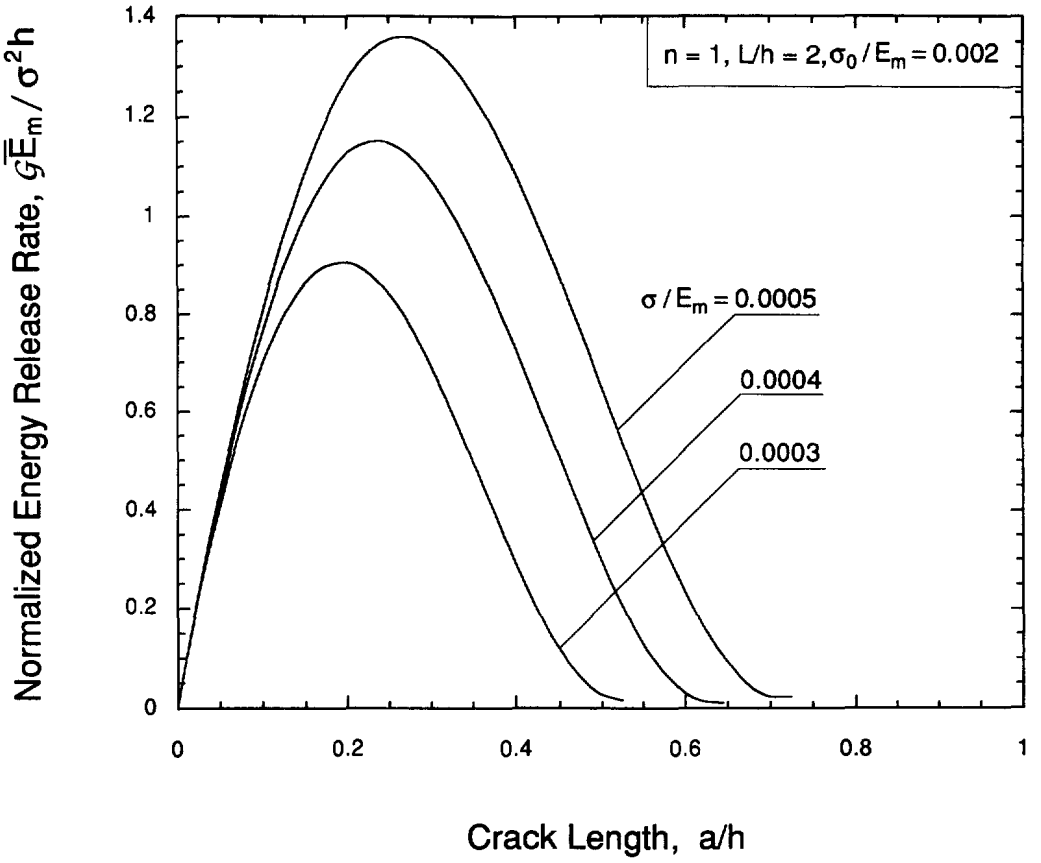

Fig. 11. The normalized energy release rate as a function of the crack length for a FGM coating with $n = 1$, $L/h = 2$, $\sigma_0/E_m = 0.002$ under applied stresses $\sigma/E_m = 0.0003$, 0.0004 and 0.0005.

4.1. *Intrinsic toughness of a FGM coating*

As a ceramic/metal composite, the toughness of a FGM coating is in general determined by the toughness of both the ceramic and the metal phases. However, compared with the metal phase, the ceramic phase in a FGM coating experiences larger stresses under a uniform applied strain field, but its toughness is much lower. Therefore, the ceramic phase in the coating always fractures first. In this study, we assume that in the ceramic-rich region of the coating, the cracks are in the ceramic matrix; metal particles contribute to the coating toughness only through crack bridging, as illustrated in Fig. 12. Further, in the metal-rich region, the crack length is so defined such that the fractured ceramic particles lying within the major crack plane are included (Fig. 12). Specifically, the crack tip is assumed to be located at the breaks of the ceramic particles, and the metal matrix in the crack plane behind the crack-tip is modeled as the bridging material. This approach is analogous to the cohesive zone model used by Rice (1968) for crack growth in a metal under small-scale yielding conditions. We thus define the *intrinsic toughness* of a FGM coating as that of the ceramic phase; the contribution of metal phase to the coating toughness is reflected by the reduction in the crack-tip energy release rate $\mathcal{G}$ due to crack bridging. From the viewpoint of energy balance concerning crack growth, both approaches, i.e., either counting bridging as a toughness enhancer or as a driving force reducer, are equivalent.

Assume that the toughness of the ceramic phase is Γ_c. For typical ceramic/metal combinations for advanced composite materials, the normalized intrinsic toughness of the coating $\Gamma_c/E_m h$ can range from 1.0×10^{-7} to 1.0×10^{-5} (Ashby and Jones, 1980). To gain insight into the stable crack growth in a FGM coating, in the following discussions, the material system consisting of SiC/Ti FGM coating on a Ti substrate will be considered as an example. Since for silicon carbide (SiC), toughness $K_c = 3$ MPa$\sqrt{\text{m}}$, Young's modulus $E_c = 450$ GPa, and for titanium (Ti), $E_m = 116$ GPa (Ashby and Jones, 1980), we have $\Gamma_c/E_m h = 1.66\times10^{-7}$ for a SiC/Ti coating with 1 mm thickness. For material systems other

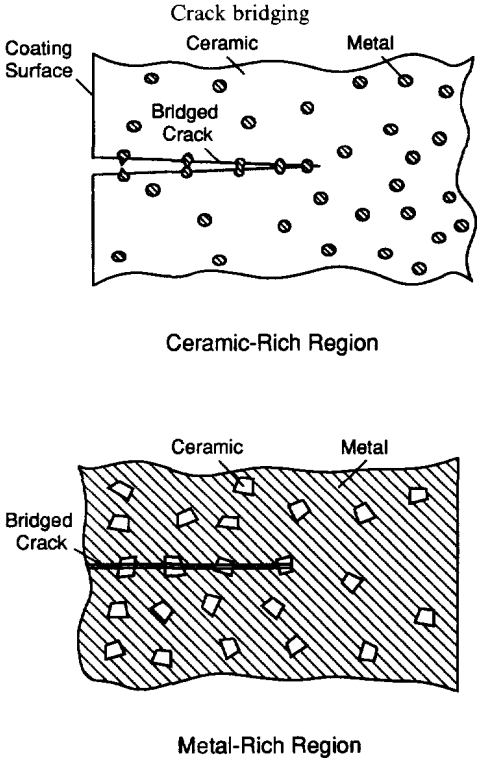

Fig. 12. A schematic showing crack bridging in different regions in the FGM coating. The crack tip is always in the ceramic phase and the intrinsic toughness of the coating is assumed to be that of the ceramic.

than the SiC/Ti considered here, the same approach can be taken in predicting the stable crack growth in a FGM coating.

4.2. *Stable crack growth in a FGM coating*

Unstable crack growth is a common feature for brittle materials such as ceramics of which the toughness is a constant independent of the crack length. However, the fracture driving force is usually a monotonic increasing function of crack length. Hence, once the crack starts to grow the whole structure or component ruptures since the fracture driving force is always higher than the toughness after the crack growth initiates at

$$\mathcal{G} = \Gamma_c \tag{20}$$

where $\mathcal{G}$ is the fracture driving force and Γ_c is the material toughness.

In contrast to unstable crack growth, stable crack growth implies that an increased applied load is necessary to propagate the crack further. For bridged multiple cracks in a FGM coating, under a given applied load, the fracture driving force $\mathcal{G}$ increases with crack length at the beginning, reaches the peak value, then decreases with crack length. Consequently, even if the crack starts to grow under a given applied load, the crack may arrest at certain crack length. Once the crack arrests, an increase in the applied load is required for further crack growth.

Shown in Fig. 13a is a typical energy release rate $\mathcal{G}\bar{E}_m/\sigma^2 h$ vs crack length a/h curve along with the intrinsic toughness of the coating $\Gamma_c\bar{E}_m/\sigma^2 h$ represented by the horizontal line, which intersects the driving force curve at crack lengths a_i and a_s. These two points have special meaning and importance: a_i corresponds to the critical initial crack length beyond which crack growth starts and a_s is the crack length at arrest. Under a given applied load, if the initial crack size is smaller than a_i the crack will not grow because the fracture driving force is lower than the toughness. On the other hand, if the initial crack size is between a_i and a_s, the crack will grow, and eventually arrest at $a = a_s$.

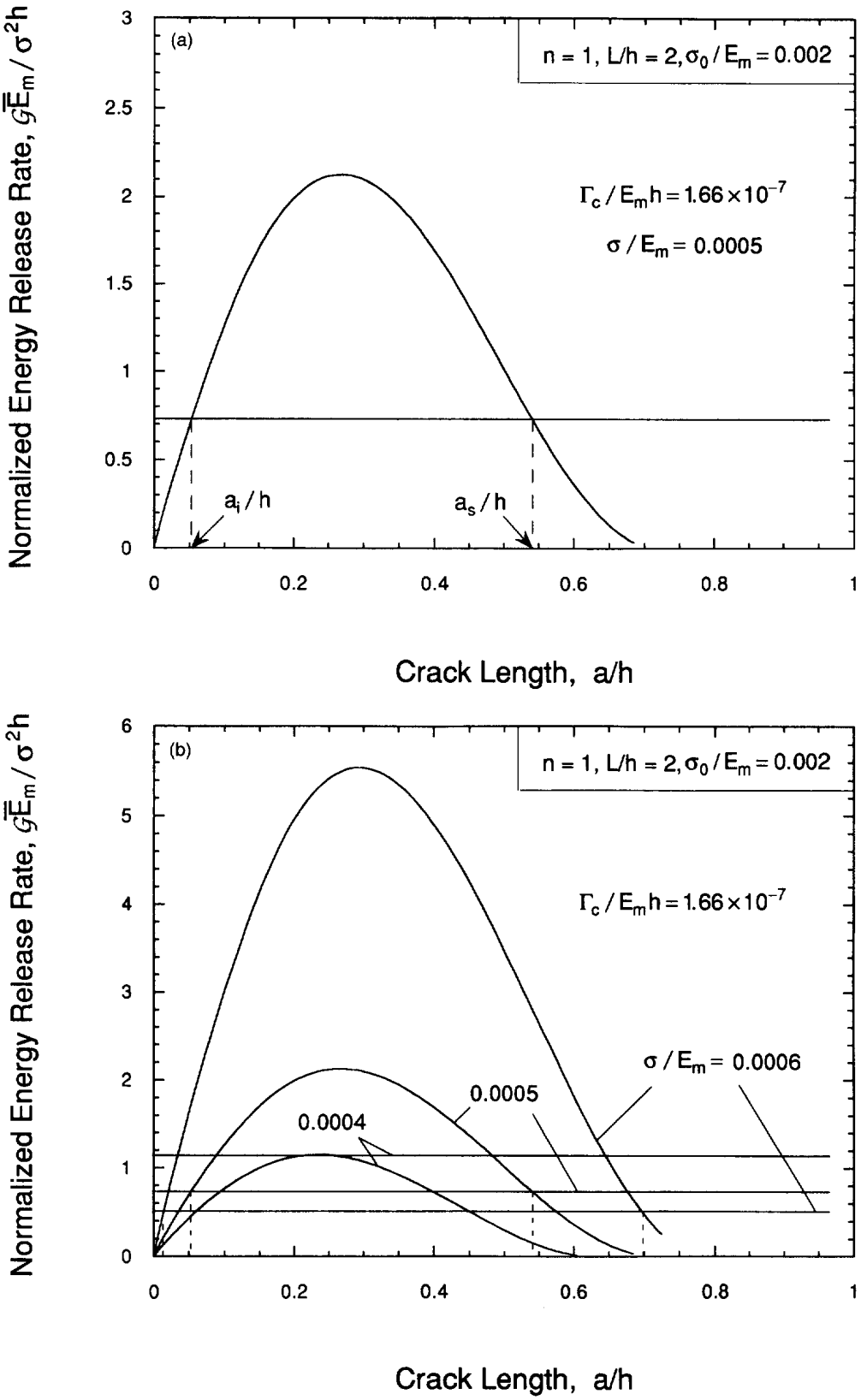

Fig. 13. Energy release rate as a function of the crack length together with the intrinsic toughness of the coating. (a) Under a given applied load, the crack starts to grow if $a \geqslant a_i$, and arrests at $a = a_s$. (b) With different applied loads, the crack has different critical initial crack length a_i and crack length at arrest a_s.

To further illustrate the trends in crack growth, in Fig. 13b curves of energy release rate $\mathscr{G}\bar{E}_m/\sigma^2 h$ vs crack length a/h are plotted together with the intrinsic toughness of the coating $\Gamma_c\bar{E}_m/\sigma^2 h$ represented by the horizontal lines for $n = 1$, $L/h = 2$, $\sigma_0/E_m = 0.002$ for $\sigma/E_m = 0.0004$, 0.0005 and 0.0006. Note that the intrinsic toughness of the coating is assumed to be $\Gamma_c/E_m h = 1.66 \times 10^{-7}$ and different horizontal lines representing $\Gamma_c\bar{E}_m/\sigma^2 h$ correspond to different values of the applied load used in calculating the energy release rate $\mathscr{G}$. Evidently, when the applied load is low, say, $\sigma/E_m = 0.0004$, the whole curve of fracture driving force $\mathscr{G}$ falls below the toughness curve Γ_c; crack growth is thus prohibited. Under a larger applied load, say, $\sigma/E_m = 0.0005$, the multiple cracks grow when their length $a \geqslant 0.05h$, and arrest at about $a = 0.54h$. At an even higher load, $\sigma/E_m = 0.0006$, the cracks start to grow at $a \approx 0.01h$ and stop at $a = 0.7h$. As expected, beyond certain crack length, further crack growth in the coating requires an increase in the applied load.

As discussed in the previous section, the fracture driving force $\mathscr{G}$ for bridged multiple cracks in the FGM coating depends on coating gradation as well as the crack bridging characteristics. In general, under a given applied load, the crack length at arrest a_s increases with decreasing n and σ_0/E_m, as can be seen from the curves in Figs 8 and 9. The influence of n and σ_0/E_m on the critical initial crack length a_i is found to be relatively insignificant.

5. CONCLUDING REMARKS

Functionally graded ceramic/metal coatings can have fracture toughness much higher than the pure ceramic coating due to the plastic deformation of the metal phase in the coating. Thus, cracks initiated at the coating surface and propagating perpendicular to the coating/substrate interface must overcome greater resistance. Specifically, in the ceramic-rich region of the coating, metal ligaments in the crack wake bridge the crack; in the metal-rich region, plastic deformation of the metal matrix near the crack tip consumes energy. To quantify the effect of crack bridging and plastic deformation on crack growth in the FGM coating, in this article, a finite element model for multiple cracking in FGM coating/metal substrate systems is developed based on a position-dependent crack bridging law. The influence of material and mechanics parameters such as coating gradation, bridging strength, crack length and spacing, and applied load on the crack tip energy release rate is studied systematically. Though relatively simple, the crack bridging analysis given in this paper can provide a basis for further studies of the fracture toughness of functionally graded materials.

The finite element results reveal that the coating gradation exponent n can have significant effects on the fracture driving force and the crack length at arrest: under fixed applied load, a larger value of n (i.e., higher metal content in the coating) gives a lower energy release rate $\mathscr{G}$ and a smaller crack length at arrest a_s. Further, with the same coating gradation, a high bridging strength σ_0 leads to a large reduction in the fracture driving force and the crack length at arrest. However, coating gradation, crack spacing, and bridging strength have very limited effects on the critical initial crack length a_i.

In this study we assume that the ductility δ_0 of the bridging material (the separation of the crack surfaces at particle rupture) and the intrinsic toughness of the coating Γ_c do not change with position in the coating. However, in reality, the crack bridging parameters σ_b and δ_0, and the intrinsic toughness Γ_c may all be position-dependent. Usually δ_0 is influenced by the size and shape of the metal particles which may change as the local volume fraction of metal in the coating varies. Further, the intrinsic toughness Γ_c—defined as the toughness of the ceramic phase—may depend on microcracking in the ceramic phase, and the thermal residual stresses. The precise position-dependence of σ_b may also be more complicated than that assumed in this article ($\sigma_b(y) = [1-(y/h)^n]\sigma_0$), since σ_0 may be different in the ceramic-rich region where the metal particles are surrounded by the ceramic matrix, and in the metal-rich region where the metal is the continuous phase. All these issues will be addressed in the subsequent studies of the fracture resistance of functionally graded materials.

The finite element crack bridging model developed in this study is based on several assumptions which render the model to be applicable only for crack lengths $a \leqslant 0.7h$. First,

the limiting separation of the crack bridging is taken to be $\delta_0 = 0.05h$ which is quite large. Consequently, in all the finite element calculations, the crack remains fully bridged. This may have overestimated the effect of crack bridging when the crack length becomes large. Further, the plastic deformation of metal in the metal-rich region of the FGM coating is taken into account through the position-dependent crack bridging law by assuming that the crack tip is located at the fractured ceramic particles in the crack plane. A consequence of this approach is that the model predictions are less accurate for crack lengths much larger than $0.6h$. This model, similar to the cohesive-zone model used by Rice (1968), is valid only if the plastic yielding is of small scale. For large-scale yielding cases, the present finite element model can be extended readily to fully reflect the effect of plastic deformation on crack growth in a FGM coating by taking the metal-rich region of the FGM coating and the metal substrate to be elastoplastic materials. Such an extension is left for future studies.

Acknowledgement—This work was supported by AFOSR through a research grant F49620-95-1-0120 to G. Bao.

REFERENCES

Aboudi, J., Arnold, S. M. and Pindera, M. J. (1994) Response of functionally graded composites to thermal gradients. *Composites Engineering* **4,** 1–18.

Ashby, M. F., Blunt, F. J. and Bannister, M. (1989) Flow characteristics of highly constrained metal wires, *Acta Metallica* **37,** 1847–1857.

Ashby, M. F. and Jones, D. R. H. (1980) *Engineering Materials* 1, Pergamon Press, New York.

Bao, G. and Cai, H. (1997) Delamination cracking in functionally graded coating/metal substrate systems. *Acta Materiala* **45,** 1055–1066.

Bao, G. and Hui, C. Y. (1990) Effects of interface debonding on the toughness of ductile-particle reinforced ceramics. *International Journal of Solids and Structures* **26,** 631–642.

Bao, G. and McMeeking, R. M. (1994) Fatigue crack growth in fiber reinforced metal matrix composites. *Acta Metallica Materiala* **42,** 2415–2425.

Bao, G. and McMeeking, R. M. (1995) Thermomechanical fatigue cracking in fiber reinforced metal-matrix composites. *Journal of the Mechanics and Physics of Solids* **43,** 1433–1460.

Bao, G. and Suo, Z. (1992) Remarks on crack bridging concepts. *Applied Mechanics Review* **45,** 355–366.

Bao, G. and Wang, L. (1995) Multiple cracking in functionally graded ceramic/metal coatings. *International Journal of Solids and Structures* **32,** 2853–2871.

Bao, G. and Zok, F. W. (1993) On the strength of ductile particle reinforced brittle matrix composites. *Acta Metallica Materiala* **41,** 3515–3524.

Chen, Y. F. and Erdogan, F. (1996) The interface crack problem for a non-homogeneous coating bonded to a homogeneous substrate. *Journal of the Mechanics and Physics of Solids* **44,** 771–787.

Christensen, R. M. and Lo, K. H. (1979) Solutions for effective shear properties in three phase sphere and cylinder models. *Journal of the Mechanics and Physics of Solids* **27,** 315–330.

Delale, F. and Erdogan, F. (1983) The crack problem for a nonhomogeneous plane. *Journal of Applied Mechanics* **50,** 609–614.

Delale, F. and Erdogan, F. (1988) On the mechanical modeling of the interface region in bonded half-planes. *Journal of Applied Mechanics* **55,** 317–324.

Drake, J. T., Williamson and Rabin, R. L., (1993) Finite element analysis of thermal residual stresses at graded ceramic-metal interfaces. Part II. Interface optimization for residual stress reduction. *Journal of Applied Physics* **74,** 1321–1326.

Dvorak, G. and Zuiker, J. (1994) The effective properties of functionally graded composites I. Extension of the Mori-Tanaka method to linearly varying fields. *Composites Engineering* **4,** 19–35.

Erdogan, F. (1985) The crack problem for bonded nonhomogeneous materials under antiplane shear loading. *Journal of Applied Mechanics* **52,** 823–828.

Erdogan, F. and Wu, B. H. (1993) Analysis of FGM specimens for fracture toughness testing. In *Ceramic Transactions*, Vol. 34: Functionally Gradient Materials, eds J. B. Hole *et al.*, pp. 39–46. American Ceramic Society, Westerville, Ohio.

Finot, M. and Suresh, S. (1996) Small and large deformation of thick and thin-film multi-layers: effects of layer geometry, plasticity and compositional gradients. *Journal of Mechanics and Physics of Solids* **44,** 683–721.

Giannakopoulos, A. E., Suresh, S., Finot, M. and Olsson, M. (1994) Elastoplastic analysis of thermal cycling: Layered materials with compositional gradients. *Acta Metallica Materiala* **43,** 1335–1354.

Hashin, Z. (1962) The elastic moduli of heterogeneous materials. *Journal of Applied Mechanics* **29,** 143–150.

Jin, Z.-H. and Noda, N. (1993) An internal crack parallel to the boundary of a nonhomogeneous half plane under thermal loading. *International Journal of Engineering Science* **31,** 793–806.

Jin, Z.-H. and Noda, N. (1994) Transient thermal stress intensity factors for a crack in a semi-infinite plate of a functionally gradient material. *International Journal of Solids and Structures* **31,** 203–218.

Kokini, K. and Takeuchi, Y. (1994) Transient thermal fracture of an interface crack in the presence of a surface crack. *Journal of Thermal Stresses* **17,** 63–74.

Lannutti, J. J. (1994) Functionally graded materials: properties, potential and design guidelines. *Composites Engineering* **4,** 81–94.

Markworth, A. J., Ramesh, K. S. and parks, W. P. Jr. (1995) Modelling studies applied to functionally graded materials. *Journal of Material Science* **30,** 2183–2193.

Mataga, P. A. (1989) Deformation of crack-bridging ductile reinforcements in tough brittle materials. *Acta Metallica* **37,** 3349.

Mortensen A. and Suresh, S. (1995) Functionally graded metals and metal-ceramic composites : Part I. Processing. *International Materials Reviews* (submitted).

Noda, N. and Jin, Z.-H. (1993) Thermal stress intensity factors for a crack in a strip of a functionally gradient material. *International Journal of Solids and Structures* **30,** 1039–1056.

Rice, J. R. (1968) Mathematical Analysis in the Mechanics of Fracture. In *Fracture—An Advanced Treatise, Vol. II,* ed. H. Liebowitz. Academic, New York, pp. 191–308.

Tada, H., Paris, P. C. and Irwin, G. R. (1985) *The Stress Analysis of Cracks Handbook.* Del Research, Hellertown, PA.

Takahashi, H. and Hashida, T. (1990) Development of an evaluation method of functionally gradient materials. *JSME International Journal* **33,** 281–287.

Walls, D. P., Bao, G. and Zok, F. W. (1993) Mode I fatigue cracking in a fiber reinforced metal matrix composite. *Acta Metallica Materiala* **41,** 2061–2071.

Williamson, R. L., Rabin, B. H. and Drake, J. T. (1993) Finite element analysis of thermal residual stresses at graded ceramic-metal interfaces. Part I. Model description and geometrical effects. *Journal of Applied Physics* **74,** 1310–1320.